Fluorescence Upconversion Properties of Er 3+ –Doped TiO 2 and BaTiO 3 Nanocrystallites

ARTICLE *in* CHEMISTRY OF MATERIALS · AUGUST 2003

Impact Factor: 8.35 · DOI: 10.1021/cm020897u

Fluorescence Upconversion Properties of Er^{3+}-Doped TiO_2 and $BaTiO_3$ Nanocrystallites

Amitava Patra, Christopher S. Friend, Rakesh Kapoor, and Paras N. Prasad*

Institute for Lasers, Photonics and Biophotonics, Department of Chemistry, University at Buffalo, The State University of New York, Buffalo, New York 14260

Received September 6, 2002. Revised Manuscript Received February 27, 2003

The effects of the erbium concentration, crystal size, crystal phase, and different processing temperatures on the upconverted emission of Er^{3+} in $BaTiO_3$ and TiO_2 nanocrystals are reported. A cw diode laser at 975 nm was used as a pump source for resonant sequential excitation of the $^4I_{11/2}$ and $^4F_{7/2}$ levels. Green and red upconversion emission at 550 and 670 nm were observed from these oxide nanocrystals with 975 nm excitation. With the same Er^{3+} concentration, the upconversion emission intensity from $BaTiO_3$ was higher than that observed in the TiO_2 host. In the TiO_2 matrix, the maximum upconversion emission intensity of Er^{3+} was found for samples calcined at 800 °C where both the anatase and the rutile phases were present. The observed emission characteristics and the pump intensity dependence of the luminescence intensity confirm that the upconverted emission in these materials is produced by two-photon excited-state absorption (ESA) processes.

Introduction

Rare-earth-doped materials find usage in a wide variety of applications, including phosphors, display monitors, X-ray imaging, scintillators, lasers, and amplifiers for fiber-optic communications.[1−3] Recently, a great deal of research on IR-to-visible frequency upconversion has been focused to find their potential applications in several areas, such as upconversion lasing, display, and two-photon imaging by confocal microscopy.[4−6] The predominant mechanisms of upconversion in these materials are excited-state absorption (ESA) and energy-transfer upconversion (ETU). In both of these cases, a simple cw diode laser can be used for the upconversion process, in contrast to expensive mode-locked lasers used for two-photon upconversion in organic fluorophore.[7] Efficient upconverting inorganic nanocrystals can be a good replacement for the organic dyes used for two-photon confocal-microscope imaging. The efficiency of these materials is dependent on the excited-state dynamics of the rare-earth ions and their interactions with the host matrix. This interaction can be a function of the host phase and the dopant concentration. The excited-state dynamics are also dependent on energy migration between the active ions, statistical distribution of the active ions, and the site symmetry of the active ions in the host matrix.[8−12] With a suitable selection of the host matrix and the rare earth dopant ion concentration, the upconversion performance of a material can be enhanced significantly. Here we report the study of the interaction of Er^{3+} with TiO_2 and $BaTiO_3$ nanocrystals, in relation to the Er^{3+} upconversion properties.

Experimental Section

The sol−emulsion−gel method was used for the preparation of Er^{3+}-doped oxide nanoparticles.[8] The flowchart in Figure 1 summarizes the synthetic approach used for the preparation of Er^{3+}-doped nanoparticles. Titanium isopropoxide, $Ti(OiPr)_4$, (Fluka) was used as the precursor for titania sol preparation. Required amounts of acetic acid (5.27 mL) and 2-butanol (135 mL) were used to prepare the sol. The requisite amount (20 mL) of titanium isopropoxide was added to half of the mixture of acetic acid and 2-butanol and the resultant sol was stirred for 30 min. Water (2.53 mL) was added to the remaining amount of the acid−alcohol mixture and the resulting solution was added dropwise

* To whom correspondence should be addressed. Phone: 716-645-6800, ext. 2098/2099. Fax: 716-645-6945. E-mail: pnprasad@acsu.buffalo.edu.

(1) Blasse, G.; Grabmaier, B. C. *Luminescent Materials*; Springer-Verlag: Berlin, 1994.
(2) Reisfeld, R.; Jorgensen, C. K *Laser and Excited State of Rare-Earths*; Reisfeld, R., Jorgensen, C. K., Eds.; Springer-Verlag: Berlin, 1977.
(3) Denjeka, M. J.; Samson, B. *Mater. Res. Soc. Bull.* **1999**, *8*, 39.
(4) Silversmith, A. J.; Lenth, W.; Macfarlane, R. M. *Appl. Phys. Lett.* **1987**, *51*, 1977.
(5) Maciel, G. S.; de Araujo, C. B.; Messaddeq, Y.; Aegerter, M. A. *Phys. Rev. B* **1997**, *55*, 6335.
(6) Kapoor, R.; Friend, C. S.; Biswas, A.; Prasad, P. N. *Opt. Lett.* **2000**, *25*, 338.
(7) Chung, S.-J.; Lin, T.-C.; Kim, K.-S.; He, G. S.; Swiatiewicz, J.; Prasad, P. N.; Baker, G. A.; Bright, F. V. *Chem. Mater.* **2001**, *13 (11)*, 4071.
(8) Patra, A.; Friend, C. S.; Kapoor, R.; Prasad, P. N. *J. Phys. Chem.* **2002**, *106*, 1909.
(9) Silver, J.; Martinez-Rubio, M. I.; Ireland, T. G.; Fern, G. R.; Withnall, R. *J. Phys. Chem. B* **2001**, *105*, 948.
(10) Newport, A.; Fern, G. R.; Ireland, T.; Withnall, R.; Silver, J.; Vecht, A. *J. Mater. Chem.* **2001**, *11*, 1447.
(11) Vetrone, F.; Boyer, J. C.; Capobianco, J. A.; Speghini, A.; Bettinelli, M. *J. Phys. Chem. B* **2002**, *106*, 5622.
(12) Bahtat, A.; Bouazaoui, M.; Bahtat, M.; Garapon, C.; Jacquier, B.; Mugnier, J. *J. Non-Cryst. Solids* **1996**, *202*, 16.

10.1021/cm020897u CCC: $25.00
Published on Web 08/19/2003

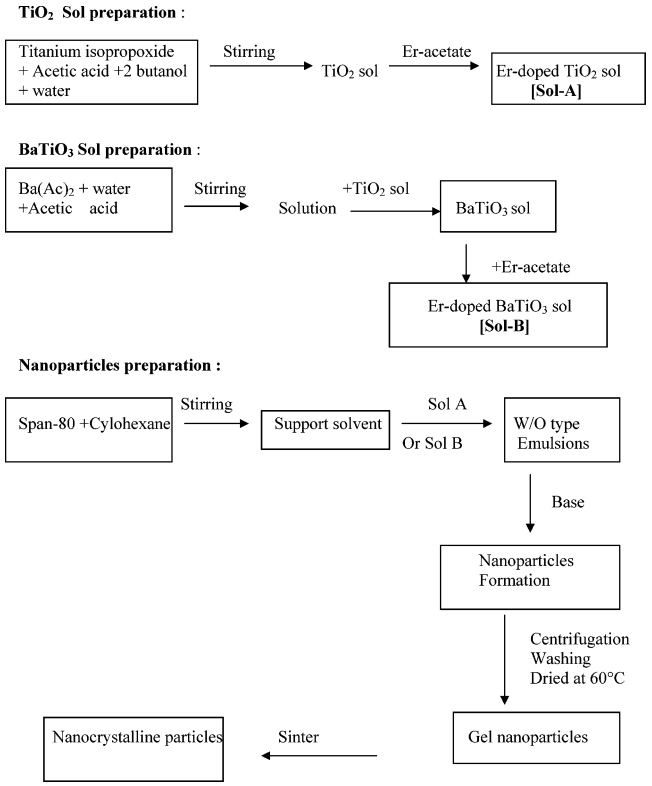

Figure 1. Processing flowchart for the synthesis of nanoparticles.

to the alkoxide−alcohol−acid mixture with stirring. The sol was then stirred for another 1 h. Then the required amount of erbium acetate was added to this sol.

Barium acetate ($Ba(CH_3COO)_2 \cdot H_2O$), titanium isopropoxide ($Ti(OiPr)_4$, from Fluka), and erbium acetate were used as the starting materials for $BaTiO_3$ sol preparation. First $Ba(Ac)_2$ was dissolved in water and acetic acid under stirring. Second, the required amount of titania sol (see above) was slowly added to this solution under vigorous stirring at ambient temperature. A clear transparent sol was thus obtained. Then the required amount of erbium acetate was added to this sol. To obtain emulsified sol droplets through water-in-oil (w/o) type emulsions, cyclohexane and sorbitan monooleate (Span 80, Fluka) were used as the organic liquid (oil phase) and the nonionic surfactant, respectively. The support solvent containing 5 vol % of Span 80 in cyclohexane was used for emulsification, i.e., for the preparation of water-in-oil (w/o) type emulsion in the present study. The volume ratio of the sol and cyclohexane was 1:4. A measured amount of the sol was then dispersed in the solvent under stirring condition. The sol droplets formed in the process were then gelled by controlled addition of a base. The gel particles were separated by centrifugation, followed by washing with acetone and methanol. The product thus obtained was dried at 60 °C in an air oven for 12 h. The dried materials were calcined at different temperatures, up to 1000 °C.

Transmission electron microscopy (TEM) was employed to determine the morphology and the particle size of the resulting powders. The crystalline phases of calcined powders were identified by X-ray diffraction (XRD). X-ray powder diffraction patterns of the different samples were recorded at a number of temperatures.

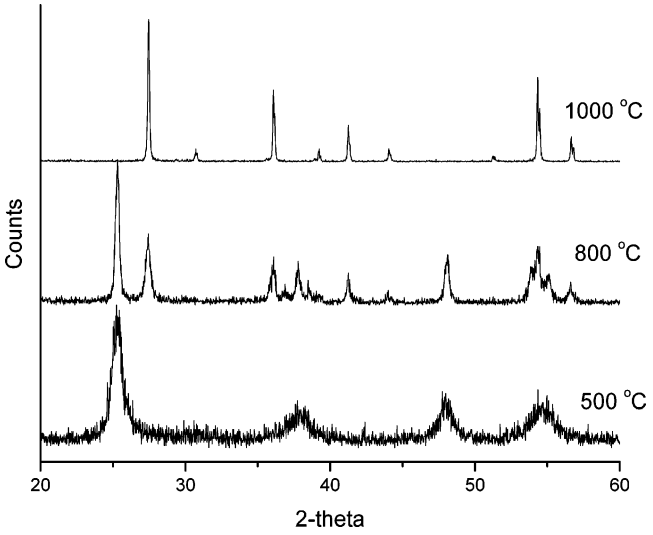

Figure 2. Powder X-ray diffraction patterns of the 0.25 mol % Er-doped TiO_2 nanoparticles prepared at three different sintering temperatures.

The crystallite sizes of the nanoparticles were also calculated using the Scherrer's equation

$$D = K\lambda/\beta\cos\Theta \quad (1)$$

where $K = 0.9$; D represents the crystallite size (Å); λ is the wavelength of Cu Kα radiation; and β is the corrected half width of the diffraction peak. We pressed the particles to form a smooth, flat disk for optical study. The samples were irradiated with a diode laser tuned to 975 nm. A CCD-coupled spectrometer recorded the fluorescence spectra. The absolute fluorescence intensity was measured with a Minolta LS-110 luminance meter.

Results and Discussion

Structural Investigations. Figure 2 represents the XRD patterns of Er^{3+}-doped TiO_2 nanocystals processed at different temperatures. It shows that only the antase phase appears at 500 °C. The anatase and the rutile phases are present in samples processed at 800 °C. The rutile phase contains a small amount of $Er_2Ti_2O_7$ crystallites when sintered at 1000 °C. The rutile phase dominates at higher temperature. Thus, the phase transformation can be controlled with annealing temperature. The crystallite size increases with the increasing temperature. Figure 3 shows the TEM picture of these particles. The estimated average crystal sizes (from TEM picture) are ∼15, 40, and >100 nm in samples processed, respectively, at 500, 800, and 1000 °C.

The powder X-ray diffraction patterns in Figure 4 indicate the crystallization of $BaTiO_3$ nanoparticles at different temperatures and the patterns show the presence of cubic phases. The crystallite size increases with an increase in the sintering temperature. At higher sintering temperatures, the small crystallite sizes grow larger; as can be seen from the TEM images of the $BaTiO_3$ nanoparticles shown in Figure 5. The estimated average crystal sizes (from TEM picture) are ∼30, 50, and >80 nm for samples processed at 700, 850, and 1000 °C, respectively.

Upconversion Properties. The energy level diagram describing the upconverted fluorescence emission

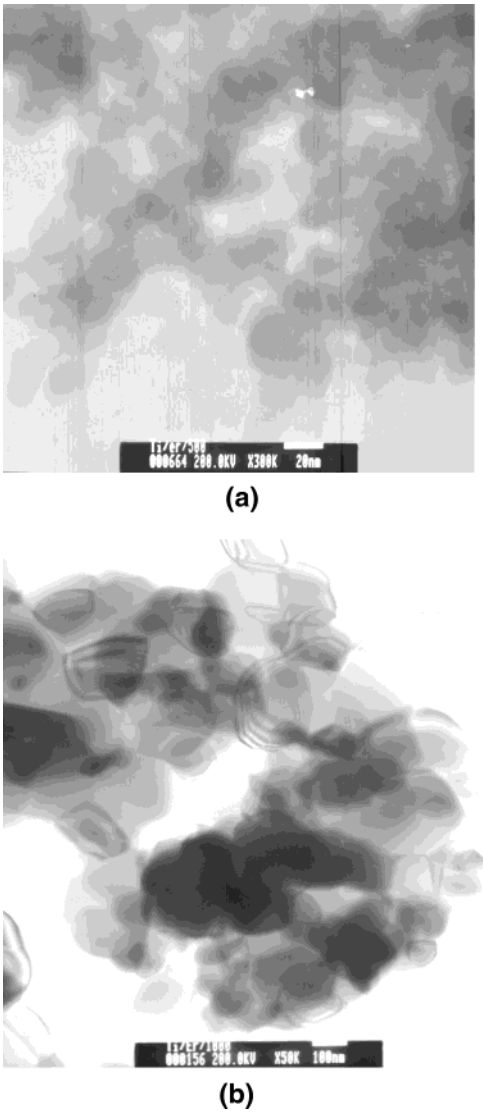

Figure 3. Transmission electron micrographs of 0.25 mol % Er^{3+}-doped TiO_2 nanoparticles obtained after sintering at different temperatures: (a) 500 °C and (b) 1000 °C.

from a sample doped with the Er^{3+} ions under infrared excitation is shown in Figure 6.

The upconverted fluorescence spectra of the Er^{3+}/TiO_2 nanocrystals at different temperatures are shown in Figure 7. The peak located near 480 nm is due to an artifact, not generated in the sample. The spectral nature of the upconversion fluorescence emission depends on the phase. Bahtat et al.[12] have already studied the upconversion fluorescence (blue, green, and red) in an Er^{3+}/TiO_2 optical planar waveguide. The anatase phase consists of TiO_6 octahedrals that share faces; whereas in the rutile phase, the TiO_6 octahedrals share only edges.[13] Therefore, the crystal field is different for the Er^{3+} ions in the different crystal phases. Hence, the nature of emission from the anatase and the rutile phases is not identical. The ionic radius value of Er^{3+} is between that of Ti^{4+} (0.068 nm) and O^{2-} (0.10 nm). Therefore the Er^{3+} could either replace some Ti^{4+} sites or go to the interstitial. The Er^{3+} ions that have replaced the Ti^{4+} sites will have a stabilizing effect on the Ti−O

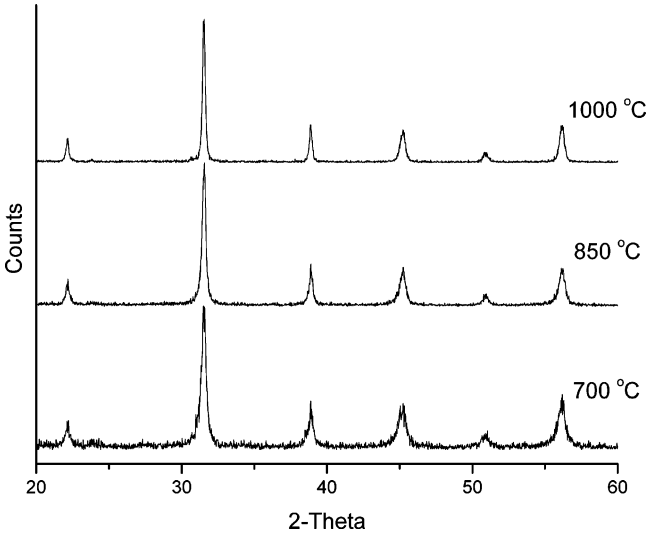

Figure 4. Powder X-ray diffraction patterns of 1.0 mol % Er-doped $BaTiO_3$ nanoparticles obtained after heating to three different temperatures.

bond because the more electropositive Er^{3+} will render its electron density to O^{2-} so that it can use this increased concentration of electrons to strengthen the bonding between O^{2-} and the less electropositive Ti^{4+} ions.[14] It is noted that the luminance value is highest for the 800 °C calcined samples where both phases are present. However, the luminance value decreases in the rutile phase present in the 1000 °C heated samples, even though the particle size increases with the increasing temperature. Newport et al.[10] also reported a similar type behavior for TiO_2-doped silica glass ceramic materials. The upconversion fluorescence spectra for the 0.25 mol % Er^{3+}/TiO_2 nanoparticles sintered at three different temperatures are shown in Figure 7. The upconversion luminance values are 97.35, 207.5, and 120.5 Cd/m^2 for the 500, 800, and 1000 °C sintering temperatures, respectively. It is clear from the absolute luminance values and the spectra shown in Figure 7 that the optimum upconversion is obtained at 800 °C when both the phases are present. Therefore, the variation of upconversion with the Er^{3+} ion concentration was recorded only for samples processed at 800 °C. It can be seen in Figure 8 that the luminance values of upconversion first increase and then decrease with an increasing concentration of the Er^{3+} ion. These results indicate that in the TiO_2 nanoparticles, the upconversion process depends not only on the crystal phase but also on the Er^{3+} concentration.

The upconverted fluorescence spectra of the $Er^{3+}/BaTiO_3$ nanocrystals calcined at 1000 °C for different concentrations of Er^{3+} are shown in Figure 9. The upconversion luminance values in the $Er^{3+}/BaTiO_3$ are 17 130, 9487, 1653, and 540 Cd/m^2 for 0.25, 1.0, 2.5, and 10 mol % Er^3, respectively. A significant drop in the overall intensity and a change in the spectral nature of these bands are observed with increasing concentration of Er^{3+} ions. Figure 10 shows the upconverted fluorescence emission spectra of the 1.0 mol % Er^3-doped $BaTiO_3$ nanoparticles prepared at three different sintering temperatures. The upconversion luminance values are 343, 1448, and 9487 Cd/m^2 for the samples made

(13) Yanagisawa, K.; Ovenstone, J. *J. Phys. Chem. B* **1999**, *103*, 7781.

(14) Reddy, B. M.; Chowdhury, B.; Smirniotis, P. G. *Appl. Catal. A* **2001**, *219* (1), 53.

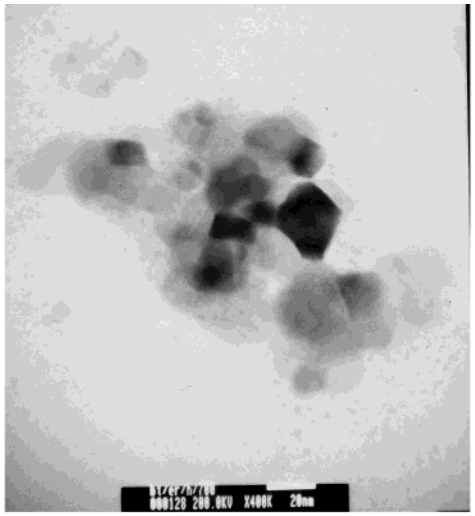

(a)

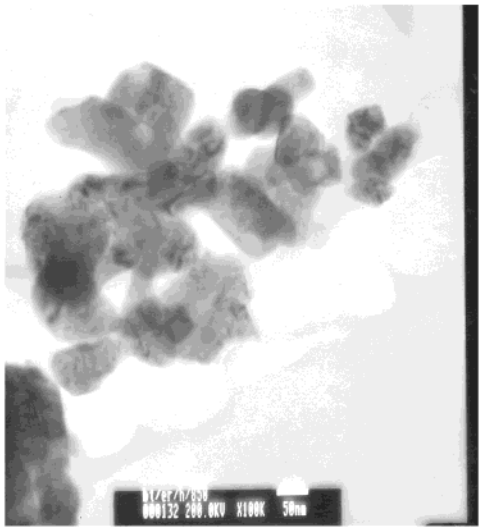

(b)

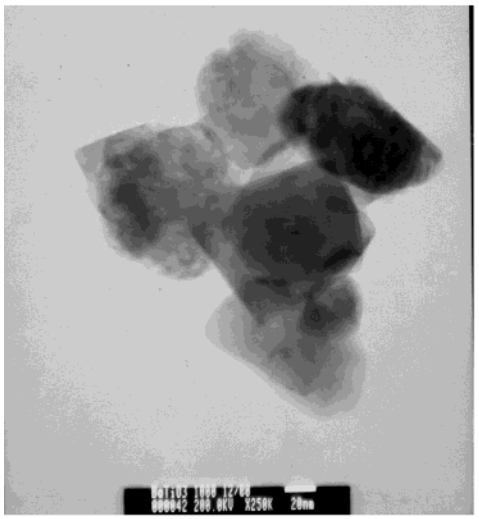

(c)

Figure 5. Transmission electron micrographs of the 1.0 mol % Er^{3+}-doped $BaTiO_3$ nanoparticles obtained after heating to three different temperatures: (a) 700 °C, (b) 850 °C, and (c) 1000 °C.

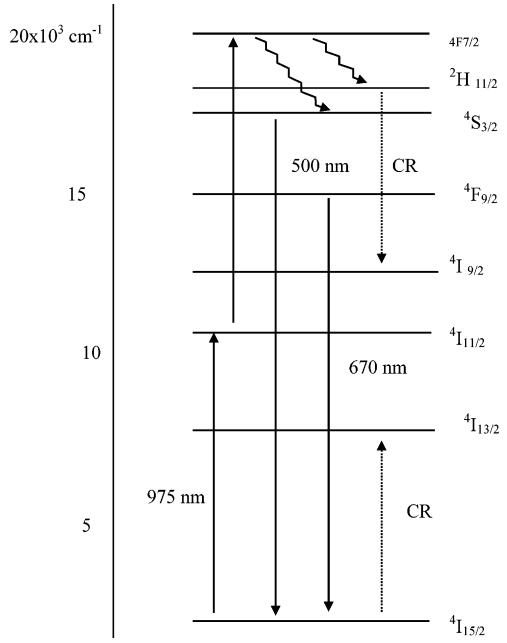

Figure 6. Energy level diagram for Er^{3+} ions, infrared excitation of 975 nm used.

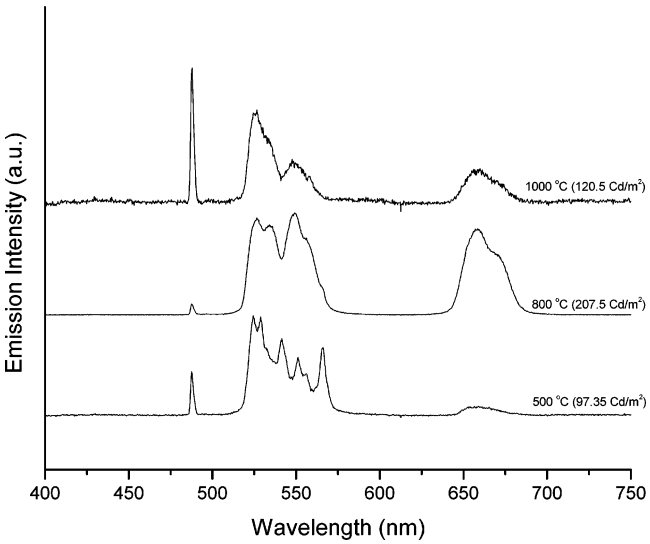

Figure 7. Upconverted fluorescence emission spectra of the 0.25 mol % Er^{3+}-doped TiO_2 nanoparticles sintered at three different temperatures.

at 700, 850, and 1000 °C sintering temperatures, respectively. In this case, we have the same crystal phase (cubic) with different temperatures, but the particles size increases with the increasing processing temperature. This indicates that the upconversion process is dependent not only on the Er^{3+} concentration but also on the particle size. As shown in Figure 5, increasing the sintering temperature yields larger nanoparticles. Considering the size of the Er^{3+} ion (~0.10 nm) is almost intermediate between those of the Ba^{2+} ion (~0.14 nm) and the Ti^{4+} ion (~0.06 nm), it seems equally likely that the Er^{3+} ions occupy the site of either ion in the $BaTiO_3$ lattice. At low concentration (0.25 mol %), the mean distance between the Er^{3+} ions is estimated by $R = 0.62/(N)^{1/3}$ to be 1.81 nm, but the distance is 0.84 nm for high concentration (2.5 mol %).[15] The erbium ions in low concentration are usually randomly distributed in the host lattice and the $Er^{3+}-Er^{3+}$

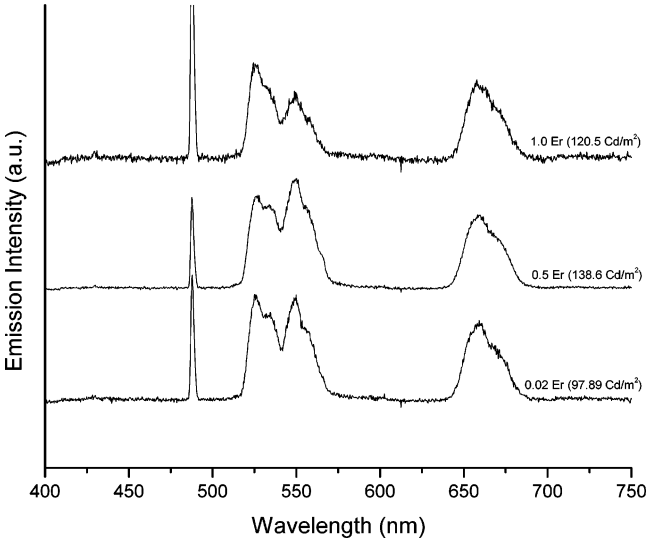

Figure 8. Upconverted fluorescence emission spectra of different concentrations of Er^{3+} in TiO_2 nanoparticles heated to 800 °C.

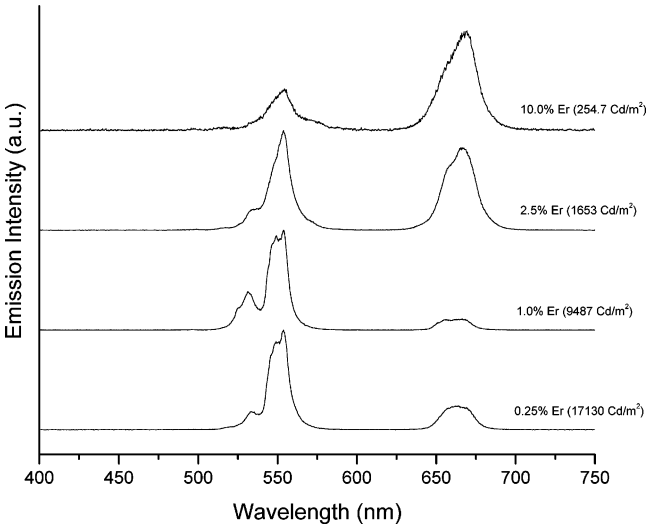

Figure 9. Upconverted fluorescence emission spectra of different concentrations of Er^{3+} in $BaTiO_3$ nanoparticles heated to 1000 °C.

distances are too far apart, but at higher concentration the distances between two Er^{3+} ions are shortening,[16] thus leading to formation of Er^{3+} clusters. As a result concentration-quenching processes will be the predominant nonradiative decay processes at higher concentrations. It is shown[17] that the probability for dopant pair-state formation depends on the size of the particles. Also, the contribution of ions at the surface sites becomes increasingly important as the size decreases. As a result, for the same concentration of dopant ions, the fraction of pairs will be different for different particles sizes. In normal crystal, the surface does not influence the statistics for pair formation because the number of nearest-neighbors is lower at the surface. However, the fraction of dopant ion-pairs for a given concentration in a very small crystal will be size

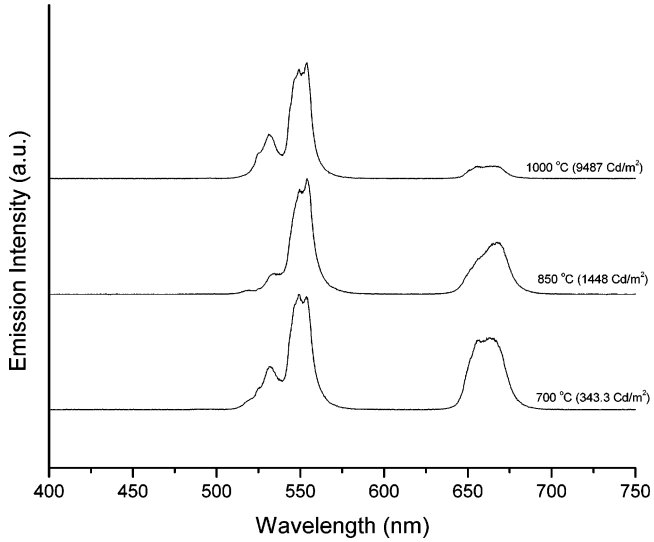

Figure 10. Upconverted fluorescence emission spectra of 1.0 mol % Er^{3+}-doped $BaTiO_3$ nanoparticles heated to three different temperatures.

dependent. Therefore, it could be the reason for an increased upconversion luminance value with the increasing size for the same concentration. Silver et al.[9] have also shown that the upconversion process is most efficient for the larger particles. However, they have suggested that resonance energy transfer is responsible for efficient upconversion in larger particles, because resonance energy transfers extends the lifetimes of the excited states of the rare-earth ions.

The intensity ratio of the green emission to that of the red emission decreases with the increasing concentration of Er^{3+} ions. For example, in the 0.25-mol % sample, the ratio becomes 3:1, whereas in the 2.5 mol % sample we obtain a ratio of 0.888:1. On the other hand, higher concentration favors the red emission. The upconversion luminance values are 120.5 and 17 130 Cd/m^2 for the 1000 °C heated 0.25 mol % Er^{3+}-doped TiO_2 and $BaTiO_3$ samples, respectively. These results can be explained from the phonon energies of this host. The stretching frequency of the TiO_2 matrix is about 641 cm^{-1}, which is higher than the phonon frequency in the $BaTiO_3$ matrix. The perovskite oxide ($BaTiO_3$) matrix has low-frequency soft transverse optical (TO) mode. The low phonon energies reduce the probability of a multiphonon nonradiative process. The presence of large energy gaps between the emitting and the terminal levels will also reduce the nonradiative decay. This reduction in nonradiative decay leads to an increase in the emission efficiency. Capobianco et al.[18] have shown bands at 1500 and 3350 cm^{-1} which are due to vibrational modes of carbonates and hydroxyl ions, respectively. They have stated that the presence of these bands in the nanocrystals influence the multiphonon relaxation process. As a result the efficiency decreases in nanocrytals compared to that in bulk. However, we have not observed any such bands at 1000 °C heat-treated samples, but very weak bands at 3424, 1637.47, and 1450 cm^{-1} are observed for the 700 °C heat-treated samples.

(15) Chen. C. Y.; Petrin, R. R.; Cyeh, D.; Sibley, W. A. *Opt. Lett.* **1989**, *14*, 432.
(16) Quimby, R. S.; Miniscalco, W. J.; Thompson, B. *J. Appl. Phys.* **1994**, *76* (6), 4472.
(17) Suyver, J. F.; Meester, R.; Kelly, J. J.; Meijerink, A. *Phys. Rev. B* **2001**, *64*, 235408.
(18) Capobianco, J. A.; Vetrone, F.; Boyer, J. C.; Speghini, A.; Bettinelli, M. *J. Phys. Chem. B* **2002**, *106*, 1181.

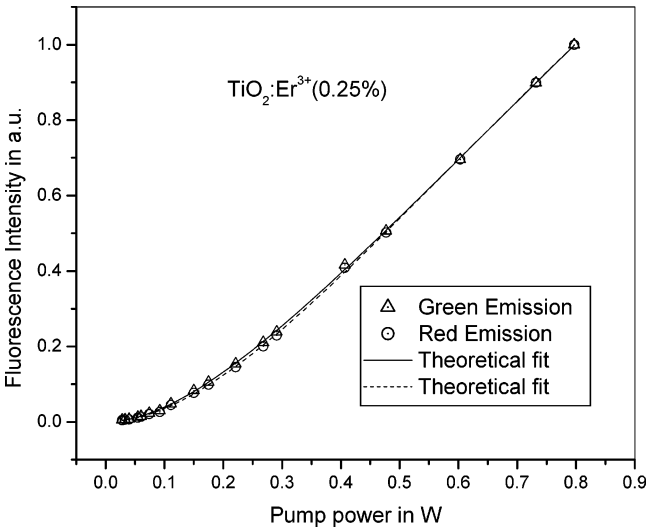

Figure 11. Variation of the red and green upconverted fluorescence emission intensities with pump power, for the 0.25 Er^{3+}/TiO_2 sample calcined at 800 °C.

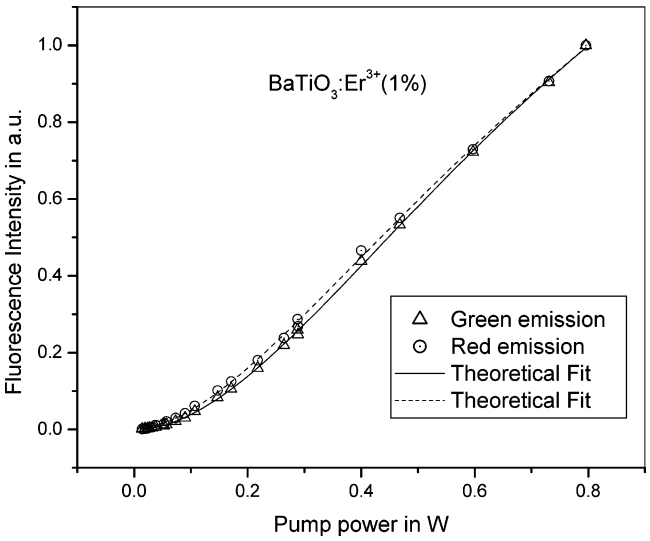

Figure 12. Variation of the red and green upconverted fluorescence emission intensities with pump power for the 1.0 $Er^{3+}/BaTiO_3$ sample calcined at 1000 °C.

The mechanism of the upconverted emission of Er^{3+} is well established in the literature.[19−22] In the ESA process, the diode-laser wavelength (975 nm) induces a transition between the ground state, $^4I_{15/2}$, and the excited level $^4I_{11/2}$. After first-level excitation, the same laser pumps the excited ion from $^4I_{11/2}$ to $^4F_{7/2}$. The$^4F_{7/2}$ (Er^{3+}) state decays nonradiatively to $^4S_{3/2}$/ $^2H_{11/2}$ and $^4F_{9/2}$ (Er^{3+}) levels. The green emission (550 nm) is observed for the $^4S_{3/2} \rightarrow {}^4I_{15/2}$ transition, while the $^4F_{9/2} \rightarrow {}^4I_{15/2}$ transition produces red emission (675 nm). At low dopant concentration, the $^4S_{3/2}/^2H_{11/2}$ levels decay mostly radiatively to $^4I_{15/2}$. Therefore, the green emission has a higher intensity. It is reported[20] that at a higher concentration, the luminescence lifetime of the $^4S_{3/2}$/ $^2H_{11/2}$ levels are shortened as a result of cross-relaxation (CR) processes between ($^2H_{11/2} \rightarrow {}^4I_{9/2}$) and ($^4I_{15/2} \rightarrow {}^4I_{13/2}$) transitions as shown in Figure 3. This cross-relaxation process is dominant at higher concentrations of Er^{3+} ions. Therefore, quenching of green emission takes place at higher concentrations of erbium ions. There is a possibility for the existence of the erbium ions at a different lattice site that prevents the aggregation, resulting in the circumvention of the nonradiative cross-relaxation process: ($^2H_{11/2} \rightarrow {}^4I_{9/2}$)/($^4I_{15/2} \rightarrow {}^4I_{13/2}$). Therefore, the $^4S_{3/2}/^2H_{11/2}$ levels decay mostly radiatively to the $^4I_{15/2}$ level and an overall increase in the green emission intensity is observed.

The intensity of the upconverted luminescence I_f is proportional to some power n of the pump intensity I_P, where n is the order of the upconversion process. The variations of the fluorescence intensity of the green and red emission versus the pump intensity for various compositions are plotted in Figures 11 and 12. For a two-photon ESA upconversion process, the fluorescence intensity should be related to the pump intensity by the following equation[6]

$$I_f = \frac{KI_p^2}{(1 + AI_p + BI_p^2)} \qquad (2)$$

where all the coefficients are always positive. I_f is the upconverted fluorescence intensity and I_P is the pumping intensity. K is a constant that depends on the collection geometry, the Er^{3+} density, and the absorption cross-section of the first and second excited states of Er^{3+}. A and B are constants related to the transition probabilities and the absorption cross-section of the involved transitions. Variations of fluorescence intensity with pump power for all the samples were recorded. Figures 11 and 12 show the curves corresponding to the most efficient upconverting samples. The theoretical fits using eq 2 are also shown in Figures 11 and 12. It can be seen that eq 2 provides an excellent fit to all sets of experimental data. These results further confirm that an ESA process is predominately responsible for upconversion in these materials.

Conclusions

We have shown that the overall upconversion luminescence intensity depends on the crystal structure, concentration, and particles size. We suggest that concentration quenching is responsible for the decrease in overall intensity at higher concentrations. For the same concentration of Er ions, a $BaTiO_3$ host showed a higher upconversion emission intensity than the TiO_2 host. In the TiO_2 matrix, the maximum upconversion emission intensity of Er^{3+} was found for the 800 °C calcined samples where both the anatase and the rutile phases were present. In the case of the $BaTiO_3$ host, the upconversion emission intensity increases with the increasing particle size. We have also confirmed that the upconversion process in all these materials involves a two-photon excited-state absorption mechanism.

Acknowledgment. This work was supported in part by an NSF grant from the Division of Materials Research and in part by a DURINT grant (F496200110358) from the Air Force Office of Scientific Research. An NSF IGERT Fellowship also supported this work.

CM020897U

(19) Auzel, F. E. *Proc. IEEE* **1973**, *61*, 758.
(20) Golding, P. S.; Jackson, S. D.; King, T. A.; Pollnau, M. *Phys. Rev. B* **2000**, *62*, 856.
(21) Pollnau, M.; Gamelin, D. R.; Luthi, S. R.; Gudel, H. U.; Hehlen, M. P. *Phys. Rev. B* **2001**, *61*, 3337.
(22) Capobianco, J. A.; Boyer, J. C.; Vetrone, F.; Speghini, A.; Bettinelli, M. *Chem. Mater.* **2002**, *14*, 2915.